

# Dynamics of magnetic flux tubes in close binary stars

## II. Nonlinear evolution and surface distributions

V. Holzwarth<sup>1,2</sup> and M. Schüssler<sup>1</sup>

<sup>1</sup> Max-Planck-Institut für Aeronomie, Max-Planck-Str. 2, 37191 Katlenburg-Lindau, Germany  
e-mail: schuessler@linmpi.mpg.de

<sup>2</sup> School of Physics and Astronomy, University of St. Andrews, North Haugh, St. Andrews KY16 9SS, UK  
e-mail: vrh1@st-andrews.ac.uk

Received gestern; accepted morgen

**Abstract.** Observations of magnetically active close binaries with orbital periods of a few days reveal the existence of starspots at preferred longitudes (with respect to the direction of the companion star). We numerically investigate the non-linear dynamics and evolution of magnetic flux tubes in the convection zone of a fast-rotating component of a close binary system and explore whether the tidal effects are able to generate non-uniformities in the surface distribution of erupting flux tubes. Assuming a synchronised system with a rotation period of two days and consisting of two solar-type components, both the tidal force and the deviation of the stellar structure from spherical shape are considered in lowest-order perturbation theory. The magnetic field is initially stored in the form of toroidal magnetic flux rings within the stably stratified overshoot region beneath the convection zone. Once the field has grown sufficiently strong, instabilities initiate the formation of rising flux loops, which rise through the convection zone and emerge at the stellar surface. We find that although the magnitude of tidal effects is rather small, they nevertheless lead to the formation of clusters of flux tube eruptions at preferred longitudes on opposite sides of the star, which result from the cumulative and resonant character of the action of tidal effects on rising flux tubes. The longitude distribution of the clusters depends on the initial parameters of flux tubes in the overshoot region like magnetic field strength and latitude, implying that there is no globally unique preferred longitude along a fixed direction.

**Key words.** binaries: close — stars: activity — stars: imaging — stars: magnetic fields — stars: spots

### 1. Introduction

Observational results indicate that in close, fast-rotating binaries like RS CVn and BY Dra systems magnetic activity is usually much more vigorous than in the case of the Sun (see, e.g., Strassmeier et al. 1993, and references therein). Data sets covering time periods much longer than the rotation period of a system reveal non-uniform longitudinal spot distributions (with respect to the direction of the companion star), which indicate the existence of long-lasting spot conglomerations at *preferred longitudes* where starspots persist longer or flux eruption is more frequent than at other surface regions (Henry et al. 1995; Jetsu 1996). The preferred longitudes are frequently about  $180^\circ$  apart on opposite sides of the stellar hemisphere (e.g., Berdyugina & Tuominen 1998; Berdyugina et al. 1998) and their dependence on rotation period, i.e., essentially on the distance between the two components, suggests that they are related to the proximity of the companion star (Heckert & Ordway 1995).

In analogy to the ‘solar paradigm’ for magnetic activity, it is assumed that starspots at the stellar surface are generated by erupting magnetic flux tubes which originate from the lower part of the outer convection zone of the star. By us-

ing non-linear numerical simulations we investigate the influence of tidal effects on the dynamics and evolution of magnetic flux tubes inside the convection zone until they erupt at the stellar surface. Particular attention is paid to the non-uniformities in the resulting surface distributions of erupting flux tubes and their dependence on initial conditions. This work complements our previous studies of the equilibrium and linear stability properties of magnetic flux tubes in the overshoot region at the lower boundary of the convection zone (Holzwarth & Schüssler 2000, 2003, hereafter HSI).

Sect. 2 contains a brief summary of the magnetic flux tube model and the analytical approximation of the close binary model. In Sect. 3 we explain the accomplishment of the numerical simulations as well as the implementation of initial conditions. Sect. 4 shows the resulting latitudinal, longitudinal and surface distributions of erupting flux tubes in the case of a binary systems with an orbital period of two days as well as a study concerning the dependence of non-uniformities on the orbital period. Sect. 5 contains a discussion of our results and Sect. 6 gives our conclusions.

## 2. Model assumptions

### 2.1. The flux tube model

We study the spot distribution on active binary stars by applying the ‘solar paradigm’ for magnetic activity, assuming that starspots are due to erupting magnetic flux tubes (e.g., Schüssler et al. 1996). In this model, the magnetic field is stored in the form of toroidal flux tubes inside the subadiabatic overshoot-region below the convection zone at the interface to the radiative core. Once a critical magnetic field strength is exceeded, perturbations initiate the onset of an undulatory (Parker-type) instability and the growth of flux loops, which rise through the convection zone and lead to the formation of bipolar active regions and starspots upon emergence at the stellar surface.

The numerical code we have used for the non-linear simulations is explicated in Moreno-Insertis (1986) and Caligari et al. (1995). All calculations are carried out in the framework of the ‘thin flux tube approximation’ (Spruit 1981) describing the evolution of an isolated magnetic flux tube embedded in a field-free environment. The surrounding convection zone is treated as an ideal plasma with vanishing viscosity and infinite conductivity, implying the concept of frozen-in magnetic fields. The dynamical interaction between the flux tube and its environment is taken into account by an hydrodynamic drag force acting upon a tube with circular cross-section which moves relative to its environment. The radius of the cross-section is determined according to the amount of magnetic flux and the lateral balance between the external gas pressure and the internal total (gas and magnetic) pressure. Since the radiative time scale in the convection zone typically exceeds the rising time of flux tubes, we assume the adiabatic evolution of flux tubes.

### 2.2. The binary model

We consider a detached binary system with two solar-type components, which move on circular orbits with an orbital period of two days. For the active star we assume synchronised, solid-body rotation, with the spin axis orientated perpendicular to the orbital plane. Its internal structure is described by a tidally deformed solar model, whereas the companion star is considered as a point mass. The model includes both the tidal force and the deviation of the stellar structure from spherical shape, which are sufficiently small to be treated in lowest-order perturbation theory (see HSI, Sect. 2.2).

Using spherical coordinates (radius  $r$ , azimuth  $\phi$ , latitude  $\lambda$ ;  $\phi = 0$  is the direction toward the companion star), the dominating term of, e.g., the azimuthal component of the effective gravitation,  $g_{\text{eff}}$ , can be written as

$$\frac{g_{\text{eff},\phi}}{g_{\star}} \sim \epsilon^3 q \sin 2\phi, \quad (1)$$

where  $g_{\star}$  is the gravitation in the unperturbed case,  $q$  is the mass ratio between the two components,  $\epsilon = (r/a)$  the expansion parameter of the approximation and  $a$  the distance between the two components. For a weakly deformed star it can be assumed that the value of any stellar quantity,  $f$ , (pressure, density, ...) is still only a function of the effective potential,

$\Psi_{\text{eff}} = \Psi_{\star} + \Psi_{\text{tide}}$ , where  $\Psi_{\star}$  is the gravitational potential of the star and  $\Psi_{\text{tide}}$  the potential of the tidal perturbation [see Eq. (2) in HSI]. Following Eq. (5) in HSI, the (Eulerian) perturbation of the stellar structure,  $\Delta f$ , can be written as

$$\frac{\Delta f}{f_{\star}} \propto \frac{\Psi_{\text{tide}}}{\Psi_{\star}} \sim \epsilon^3 q \frac{r}{H_f} \cos 2\phi, \quad (2)$$

where the undisturbed value,  $f_{\star}$ , and its local scale height,  $H_f$ , are determined from an unperturbed stellar model. The leading orders of the tidal effects given in Eqs. (1) and (2), respectively, both show a  $\pi$ -periodicity in the azimuthal direction  $\phi$ .

Using Kepler’s third law, the order of magnitude of tidal effects becomes

$$\epsilon^3 q \sim 10^{-2} \frac{q}{1+q} \left(\frac{r}{R_{\odot}}\right)^3 \left(\frac{M_{\star}}{M_{\odot}}\right)^{-1} \left(\frac{T}{\text{d}}\right)^{-2}, \quad (3)$$

while owing to the ratio  $r/H_f$  in Eq. (2), the perturbation of the stellar structure also depends on the scale height of the considered quantity. It is enhanced if  $f$  changes in a relative small stellar layer, like the superadiabaticity,  $\delta = \nabla - \nabla_{\text{ad}}$ , inside the thin overshoot region below the convection zone. For the system considered here ( $T = 2$  d,  $M_{\star} = M_{\odot}$ ,  $q = 1$  and  $r \leq R_{\odot}$ ), Eq. (3) yields  $\epsilon^3 q \sim 10^{-3}$  (with  $a \sim 8 R_{\odot}$ ).

## 3. Simulations

The linear stability analysis in HSI describes the response of a toroidal equilibrium flux tube to small perturbations inside the overshoot region and its evolution prior to its penetration to the convection zone above. In the evolution of rapidly rising flux loops in the superadiabatic region non-linear effects of the tube dynamics become important, which have to be followed by numerical simulations. According to the results in HSI, we consider flux tubes with initial magnetic field strengths between  $7 \cdot 10^4 \text{ G} \leq B_s \leq 2 \cdot 10^5 \text{ G}$ . The initial flux rings are located in the middle of the overshoot region at latitudes between  $0^\circ \leq \lambda_s \leq 80^\circ$  parallel to the equatorial plane and liable to an undulatory (Parker-type) instability (e.g., Ferriz-Mas & Schüssler 1995). The simulations start with a perturbation of a flux ring and cover up to 32 yrs of its evolution in the convection zone. In order to sample the influence of tidal effects on rising flux tubes, we carry out a large number of simulations in which each tube is subject to a perturbation localised around a different longitude,  $\phi_s$ . This is realised by an in-phase superposition of sinusoidal displacements,  $\sin m\phi$ , with azimuthal wave numbers  $m = 1 \dots 5$  and amplitudes of one percent of the local pressure scale height (Fig. 1). For simulations pertaining to a given  $(B_s, \lambda_s)$  configuration, this specific perturbation is successively shifted in longitude; the interval  $0 \leq \phi_s < 180^\circ$  is sampled with 20 simulations, each separated by  $\Delta\lambda_s = 9^\circ$ . Owing to the azimuthal  $\pi$ -periodicity of the underlying problem, the resulting pattern of flux tube emergence is then extended to the interval  $180^\circ \leq \phi_s < 360^\circ$ . The regularly distributed positions  $(\lambda_s, \phi_s)$  of the localised perturbations are shown as points in the polar projection of the overshoot region in the left panel of Fig. 2. The evolution of rising flux tubes is followed close to their eruption at the stellar surface, resulting

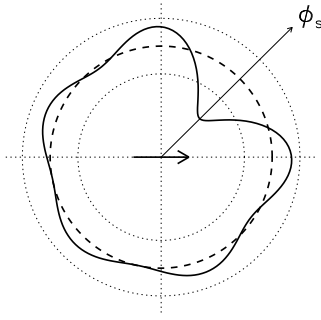


**Fig. 1.** Schematic illustration of the initial ‘localised perturbation’ of a flux ring (*dashed*) resulting from the in-phase superposition of sinusoidal wave modes with  $m = 1 \dots 5$ . The perturbation is largest around the longitude  $\phi_s$ . The central arrow indicates the direction toward the companion star.

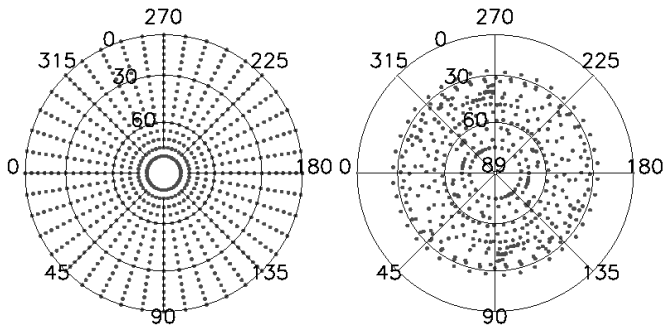


**Fig. 2.** Polar projections showing the overshoot region with the uniformly distributed positions  $(\lambda_s, \phi_s)$  of initial perturbations (*left*) and a surface distribution with the positions  $(\lambda_e, \phi_e)$  of erupting flux tubes resulting from their non-linear evolution in the convection zone (*right*). In this example with  $B_s = 1.2 \cdot 10^5$  G preferred longitudes are discernable at intermediate latitudes  $\lambda_e \sim 45^\circ$  near the quadrature longitudes; a number of flux tubes do not emerge due to their stable initial configuration. The star rotates in counter-clockwise direction and the companion star is located in the direction  $\phi = 0$ .

in spot distributions  $(\lambda_e, \phi_e)$  like the example shown in the right panel of Fig. 2. A complete set of simulations represents a non-linear mapping from the bottom of the convection zone to the top, assuming uniform distributions for the perturbations over longitude and for the flux rings over latitude in the overshoot region. The simulations stop at about  $0.98 R_\odot$ , where the ‘thin flux tube approximation’ ceases to be valid. Since the rise of the tube’s crest through the uppermost parts of the convection zone is very fast and nearly radial, there is hardly a difference between its final position in the simulation and the position of eruption at the stellar surface.

A toroidal isentropic flux tube embedded in the tidally distorted stratification of a binary star actually represents a non-equilibrium configuration, since it exhibits a density contrast along the tube axis which entails a small deviation from mechanical equilibrium. Following the linear stability analysis in HSI, the dynamical tube evolution due to this azimuthal density variation proceeds on very long time scales of several thousand

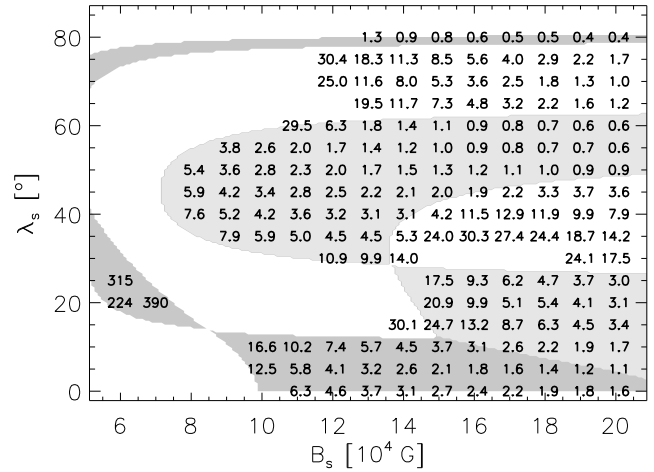


**Fig. 3.** Eruption times  $t_e$  in years, where the position  $(B_s, \lambda_s)$  in the diagram refers to the initial flux tube configuration in the overshoot region. According to the linear stability analysis in HSI, grey shaded regions mark domains of Parker-type instabilities with dominating azimuthal wave numbers  $m = 1$  (*dark*) and  $m = 2$  (*light*). Configurations in white regions are linearly stable, but yield eruptions due to the non-linear flow instability.

days, which are not relevant for the eruption of magnetic flux at the stellar surface. Since the perturbation of the flux tube due to the density variation along the tube is much smaller than the perturbation arising from the superimposed displacement (described above) and furthermore identical for all simulations at a given latitude, its effect, if any, on the longitudinal distribution of erupting flux tubes is expected to be neglectable.

## 4. Results

### 4.1. Eruption times

The eruption times,  $t_e$ , defined as the elapsed time between the initial perturbation of a flux tube and its emergence at the stellar surface, are found to be of the order of several months to years, in a few cases (near the instability boundaries) up to decades. Their dependence on the initial  $(B_s, \lambda_s)$  configurations (Fig. 3) is roughly proportional to the respective growth times of the linear instability in the overshoot region, which are, according to the analysis in HSI, dominated by Parker-type instabilities with azimuthal wave numbers  $m = 1$  and 2. On the other hand, flux tubes in linearly stable initial configurations, e.g., at  $\lambda_s \approx 65 \dots 75^\circ$  or in the stability island at intermediate latitudes and high field strengths, are found to become unstable by another mechanism, which we ascribe to the interaction of a flux tubes with the environment due to its hydrodynamic drag once the relative tangential flow velocity exceeds the phase velocity of a perturbation; a detailed description of this flow instability will be given in a subsequent paper. This second-order effect is not included in the framework of the linear stability analysis in HSI, but nevertheless appears in the course of non-linear simulations and leads to the formation of rising flux tubes on time scales comparable to those of the Parker-type instability. At high magnetic field strengths this instability mechanism con-

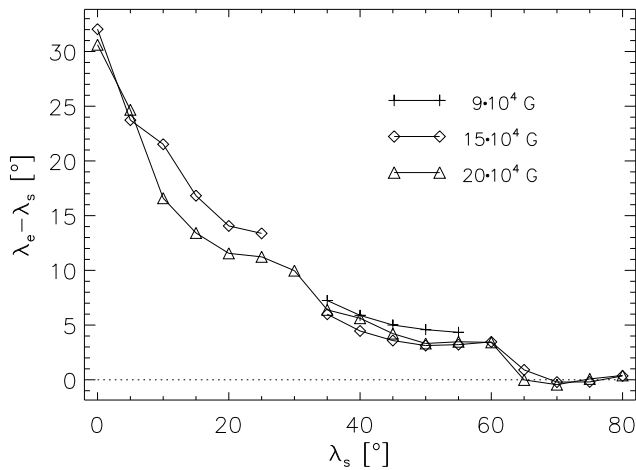


**Fig. 4.** Poleward deflection,  $\Delta\lambda = \lambda_e - \lambda_s$ , of erupting flux tubes as a function of their initial latitude  $\lambda_s$  in the overshoot region. Symbols mark different initial field strengths,  $B_s$ .

tributes a substantial fraction to the total number of erupting flux tubes. In contrast, simulations with initial configurations in the instability islands at low field strengths and  $\lambda_s \sim 20^\circ$  result in eruption times of several hundred years and thus are probably irrelevant.

The simulated rise of flux tubes through the convection zone does not always proceed in a continuous manner. Some flux tubes become unstable and form rising loops in the overshoot region, but then pass through a dynamical stage of quasi-stability where their radial rise temporarily comes to a halt before they resume after some several hundred days their ascent through the convection zone toward the surface.

#### 4.2. Latitudinal distributions

Whereas sunspots exclusively appear in an equatorial belt between about  $\pm 35^\circ$  latitude, fast-rotating stars frequently show spots also at intermediate, high, and even polar latitudes. In the framework of the magnetic flux tube model, this behaviour is explained by the influence of the Coriolis force, which acts on the internal gas flow along the tube axis and causes a poleward deflection of the tube (Schüssler & Solanki 1992). Figure 4 shows the latitude excursion,  $\Delta\lambda = \lambda_e - \lambda_s$ , i.e., the difference between the latitude of emergence,  $\lambda_e$ , and the starting latitude in the overshoot region, for flux tubes with different initial magnetic field strengths,  $B_s$ . The deflection is largest for flux tubes starting at low latitudes. It decreases considerably with increasing  $\lambda_s$  and eventually drops to zero at high latitudes. Flux tubes starting above  $\lambda_s \gtrsim 60^\circ$  essentially do not show any deflection. The poleward deflection depends only marginally on the initial magnetic field strength. At moderate latitudes,  $\Delta\lambda$  becomes somewhat smaller for increasing  $B_s$ , because the larger buoyancy force leads to a more radial rise through the convection zone.

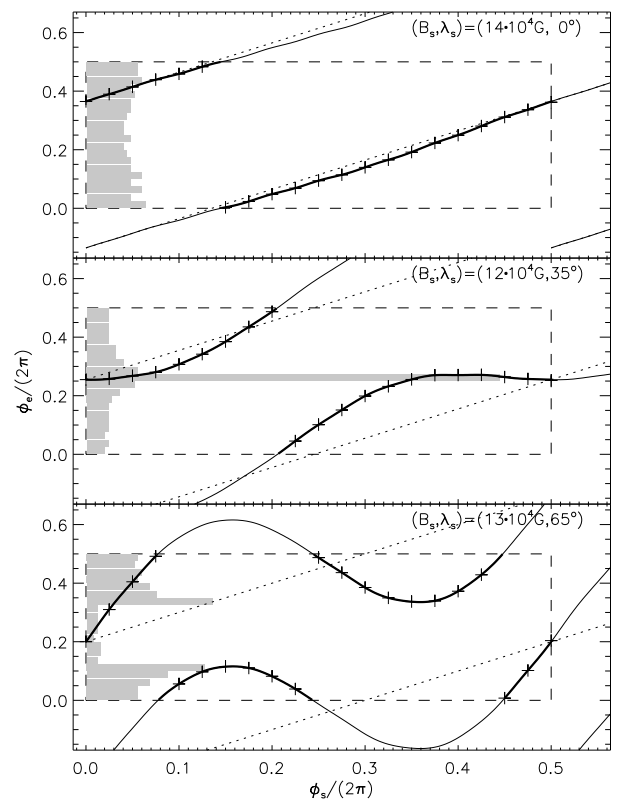


**Fig. 5.** Distributions of eruption longitudes,  $\phi_e$ , as a function of the initial perturbation longitude,  $\phi_s$ . Crosses mark the results of simulations, solid lines the (interpolated) non-linear functions  $\phi_e(\phi_s)$  in the binary problem, and dotted lines the linear functions in the corresponding single star problem. The grey histograms at the left side show the resulting distributions of erupting flux tubes binned to  $9^\circ$ -wide longitudinal intervals (abscissa gives normalised values). The distributions show (from *top to bottom*) a rather flat distribution, a clearly preferred longitude, and a favoured longitude range for emergence, respectively.

#### 4.3. Longitudinal distributions

Figure 5 shows examples of longitudinal distributions of erupting flux tubes in a binary star. Owing to the wave-like character of the instability, the longitude of emergence,  $\phi_e$ , differs from the formation longitude of a rising loop in the overshoot region. In a single star, an azimuthal shift of the localised perturbation by an offset  $\Delta\phi_s$  yields the same offset in the longitude of emergence. Under the action of tidal forces in a deformed binary star, however, the dynamics and evolution of a flux tube depend on the value of  $\phi_s$ . The longitudes of emergence thus exhibit a deviation from the uniform distribution for a single star, with the amplitude of the  $\pi$ -periodic deviation depending on the  $(B_s, \lambda_s)$  values of the initial flux ring. This results in a non-uniform longitudinal distribution of erupting flux tubes (represented in Fig. 5 by the histograms at the left side of each panel), which show clear indications for preferred longitude ranges of flux eruption: beside cases with only marginal, if any, longitudinal non-uniformity, there are cases of highly

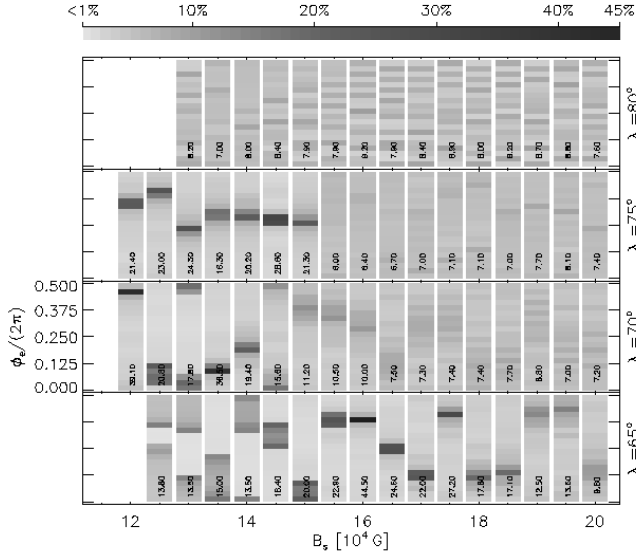


**Fig. 6.** Longitudinal distributions of erupting flux tubes with high initial latitudes,  $\lambda_s = 65 \dots 80^\circ$ . The shading indicates the amount of clustering inside  $9^\circ$ -wide longitudinal intervals normalised to the total number of flux tubes for each parameter pair  $(B_s, \lambda_s)$ ; the numbers give the maximum values for each case. Because of the  $\pi$ -periodicity in longitude, only the range  $0 \leq \phi_c/(2\pi) < .5$  is shown. White regions indicate stable, non-erupting flux tubes.

peaked distributions as well as distributions where a broad longitudinal interval is preferred.

#### 4.3.1. High latitudes ( $\lambda_s = 65 \dots 80^\circ$ )

Figure 6 shows the longitudinal patterns of emergence for high initial latitudes, based on the corresponding histogram for each  $(B_s, \lambda_s)$  configuration. The shading indicates the amount of longitudinal clustering of erupting flux tubes. For  $\lambda_s \approx 80^\circ$  we have Parker-type instabilities with the azimuthal wave number  $m = 1$  and almost flat distributions in longitude. For latitudes between  $\lambda_s \approx 65 \dots 75^\circ$  and moderate field strengths considerable asymmetries appear in the form of highly peaked distributions or broad preferred intervals. In some cases, up to 45% of all flux tubes of a  $(B_s, \lambda_s)$  configuration emerge within a longitude interval of only  $9^\circ$  width. Apart from a decreasing tendency for clustering with increasing field strength, there is no concise systematic dependency of the longitude distribution of these features on the initial  $(B_s, \lambda_s)$  parameters.

#### 4.3.2. Intermediate latitudes ( $\lambda_s = 30 \dots 60^\circ$ )

The evolution of flux tubes starting at intermediate latitudes are significantly affected by tidal effects. Figure 7 shows longitudinal distributions of erupting flux tubes starting between  $\lambda_s = 30 \dots 60^\circ$  in the overshoot region. In the domain of Parker-type instabilities with the azimuthal wave number  $m = 2$  (left to the vertical black lines), the concentration and orientation of clusters of emerging flux tubes depends systematically on the

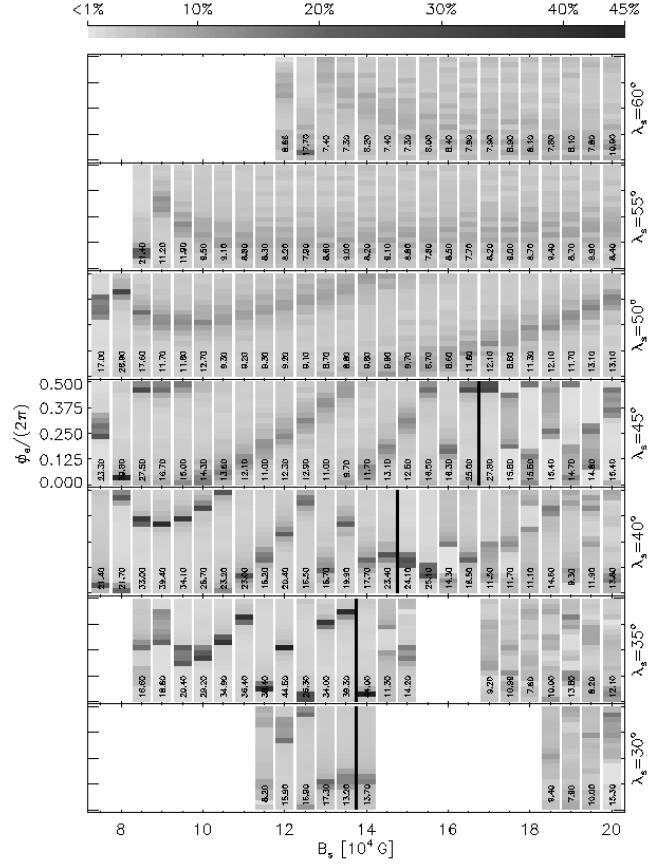


**Fig. 7.** Longitudinal distributions of erupting flux tubes with intermediate initial latitudes  $\lambda_s = 30 \dots 60^\circ$ . The vertical black lines divide the domains of linear instabilities according to HSI: the upper left domain is dominated by Parker-type instabilities with  $m = 2$ , whereas the region to the right shows the flow instability. White regions indicate stable, non-erupting flux tubes.

initial values  $(B_s, \lambda_s)$ . The most prominent clusters occur for  $\lambda_s \approx 35 \dots 40^\circ$  and  $B_s \approx 8 \dots 14 \cdot 10^4$  G. An important aspect is the orientation of preferred longitudes with respect to the direction of the companion star at  $\phi = 0$ . Figure 7 shows that clusters basically show up at all orientations depending on the initial configuration. Since there is no unique orientation for all configurations we use the term *preferred longitude* in relation to the clustering of erupting tubes for an individual  $(B_s, \lambda_s)$  configuration. For increasing magnetic field strength near the instability threshold, the clusters are shifted toward smaller longitudes (retrograde with respect to the rotation of the system), whereas for high  $B_s$  this trend reverses and the clusters shift toward larger longitudes (prograde). The slope of this longitudinal shift as a function of field strength depends on the starting latitude of the tube. At small  $\lambda_s$ , the slope is rather large and an increase of  $B_s$  by about  $5 \cdot 10^3$  G can result in an azimuthal shift of the cluster by  $90^\circ$ . The slope decreases considerably with increasing starting latitude and approaches zero at  $\lambda_s \approx 55^\circ$ . Here the orientation of clusters is apparently independent of the magnetic field strength, thus representing a kind of *fixed* preferred longitudes. However, in this case the clustering is rather weak. The shift rate seems to be related to the

amount of clustering, with more concentrated clusters showing larger shift rates.

#### 4.3.3. Low latitudes ( $\lambda_s = 0 \dots 25^\circ$ )

Longitudinal distributions of erupting flux tubes starting at equatorial latitudes ( $\lambda_s \leq 10^\circ$ ) and liable to the Parker-type instability with wave number  $m = 1$  do not show significant non-uniformities. For  $\lambda_s = 15 \dots 25^\circ$ , flux tubes become unstable above  $B_s \approx 1.4 \cdot 10^5$  G with the dominating wave mode  $m = 2$ . This domain of initial configurations is characterised by a particular evolutionary behaviour: flux tubes with the same ( $B_s, \lambda_s$ ) do not exhibit a systematic continuous dependence of the emergence longitude on  $\phi_s$  like in Fig. 5, but an irregular distribution. This aspect of the simulation results is discussed in more detail in Sect. 5.

#### 4.4. Surface distributions

Figure 8 shows polar projections of the surface distributions of erupting flux tubes with different initial field strengths,  $B_s$ , combining both longitudinal and latitudinal information with the grid of simulations  $(\Delta\phi_s, \Delta\lambda_s) = (9^\circ, 5^\circ)$  shown in the left panel of Fig. 2. Owing to the poleward deflection and the azimuthal non-uniformities induced by tidal effects, the surface distributions deviate considerably from the uniform distribution of initial flux tubes at the bottom of the convection zone and typically show features on opposite sides of the stellar hemisphere resulting from the dominating  $\pi$ -periodicity of tidal effects. While some parts of the surface are avoided by erupting flux tubes, like the equatorial belt below about  $25^\circ$ , they gather in other regions to form clusters of flux eruption. For low magnetic field strengths, only a few flux tubes starting from intermediate latitudes reach the surface, whereas the majority of tubes at other latitudes does not leave the overshoot region owing to their stable initial configuration. For increasing field strengths more flux tubes become unstable and contribute to the overall surface pattern erupting particularly at moderate and high latitudes. The flux eruption at high latitudes is mainly due to the flow instability, which results in clusters, if any, covering broad longitudinal intervals. Flux tubes erupting at moderate latitudes are due to Parker-type instabilities with wave number  $m = 1$  starting at low initial latitudes. These configurations hardly show longitudinal asymmetries. However, flux tubes starting at somewhat higher latitudes with  $m = 2$  experience a smaller poleward deflection and emerge at moderate latitudes, too, showing considerably non-uniform longitudinal distributions. At intermediate latitudes and high field strengths the extended and less pronounced clusters are due to the flow instability. The systematic dependence of preferred longitudes, which is discernible in the distributions shown in Fig. 7, is less evident in the surface patterns, because, owing to the variable poleward deflection, flux tubes from different initial latitudes emerge in the same surface area. Since the orientation of clusters in distributions with the same field strength  $B_s$  but different latitudes  $\lambda_s$  are usually not the same, their superposition in the surface pattern sometimes leads to broader emergence patterns.

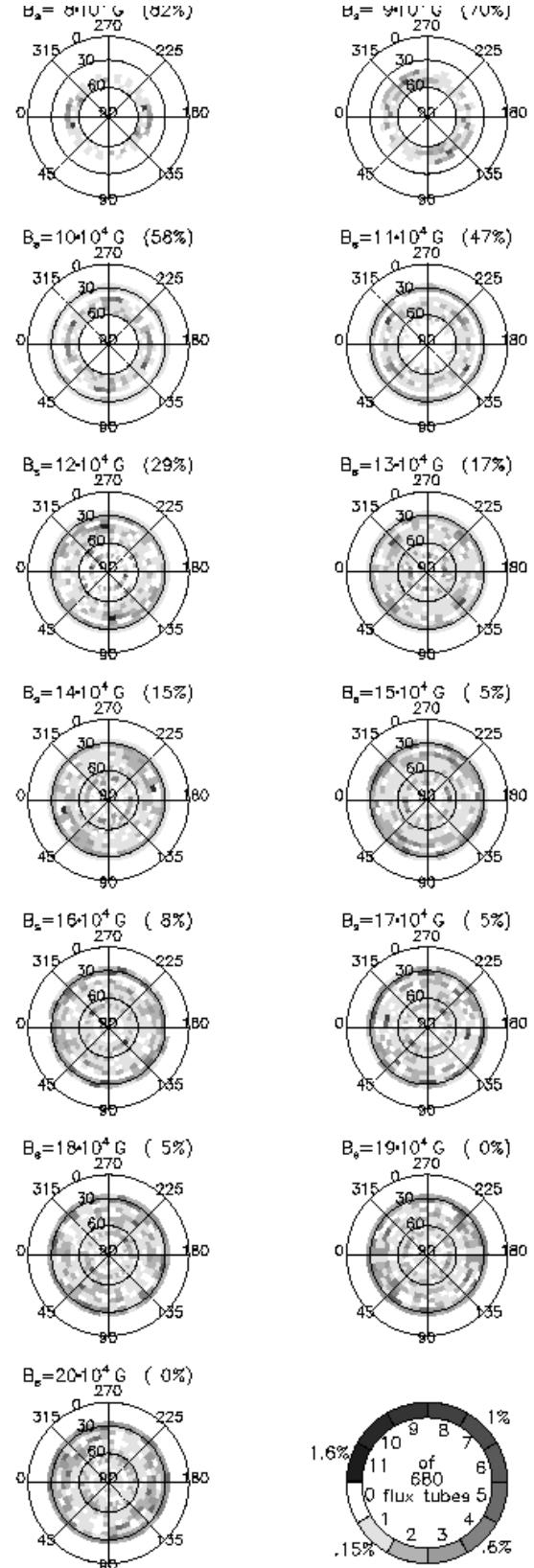


**Fig. 8.** Surface distributions of erupting flux tubes for different initial field strengths,  $B_s$ . The star rotates in counter-clockwise direction,  $\phi = 0$  is the direction toward the companion star. The shading indicates the number of flux tubes erupting in a  $(\Delta\phi_e, \Delta\lambda_e) = (9^\circ, 5^\circ)$ -wide surface area. The values in brackets give the relative number of flux tubes which do not erupt at the surface due to their stable equilibrium in the overshoot region.

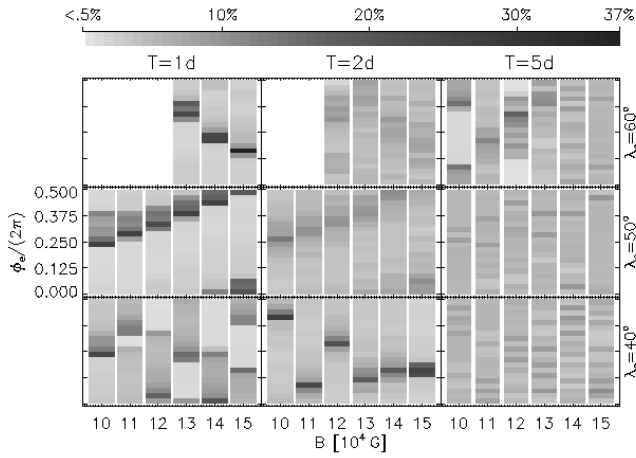


**Fig. 9.** Longitudinal distributions of erupting flux tube for systems with orbital periods  $T = 1, 2$  and  $5$  d (from left to right). Shown are distributions for flux tubes starting at intermediate latitudes.

However, particularly at low field strengths, the existence of considerable clusters at preferred longitudes remain, while for higher field strengths significant non-uniformities are still discernible in the overall surface patterns.

#### 4.5. Dependence on system period

We have investigated the influence of the magnitude of the tidal effects by considering systems with orbital periods  $T = 1$  d and  $5$  d, which correspond to binary separations  $a = 5.3 R_{\odot}$  and  $15.5 R_{\odot}$ , respectively. Figure 9 shows a comparison of longitudinal distributions of eruption for flux tubes with intermediate initial latitudes and field strengths  $B_s = 1 \dots 1.5 \cdot 10^5$  G. In the case  $T = 5$  d, most longitudinal distributions show hardly any significant clusters of eruption. Merely for  $\lambda_s = 60^\circ$  there are some non-uniformities, which indicate that tidal effects can still be effective for some initial tube configurations. The case  $T = 2$  d, the reference case discussed in detail above, shows the existence of considerable emergence clusters and the systematic dependence of their orientation on the initial tube configuration. For the shorter orbital period  $T = 1$  d the degree of clustering increases. However, for some initial tube configurations there is a transition from highly peaked distributions toward more extended preferred intervals. In contrast to highly peaked clusters these patterns of eruption are rather characterised by an avoidance of certain longitudinal intervals.

## 5. Discussion

Our results show that the presence of the companion star in a close binary system can considerably alter the evolution and surface distribution of erupting magnetic flux tubes. The actual influence of tidal effects on a rising flux tube depends on its initial magnetic field strength,  $B_s$ , and latitude,  $\lambda_s$ . This includes the stability properties of the initial flux ring in the overshoot region, i.e., the instability mechanism and the azimuthal wave number,  $m$ , of the dominating unstable eigenmode, which gov-

erns the character of the subsequent non-linear evolution. In our range of parameters, only single-loop tubes (with  $m = 1$ ) and double-loop tubes (with  $m = 2$ ) appear.

The properties of erupting flux tubes can roughly be classified according to their linear instability mechanism as determined in HSI. In the domain of Parker-type instabilities, erupting single-loop tubes starting at either low or very high latitudes tend to form uniform longitudinal patterns of eruption, whereas double-loop tubes result in clusters of eruption concentrated in narrow longitudinal intervals. This specific behaviour is presumably due to the congruency between the double-loop geometry of the rising tube and the  $\pi$ -periodicity of the tidal effects, which enables a *resonant* interaction. Although there is no globally unique orientation for the clusters of eruption, the longitudinal shift of the clusters (usually prograde with increasing  $B_s$ ) can become very small and even vanish leading to *fixed* preferred longitudes at a certain latitude. Tubes erupting due to the flow instability show a strong susceptibility to tidal effects leading to extended preferred intervals. In contrast to the domain of the Parker-type instability with  $m = 2$ , the orientations of the preferred intervals in this case lack a systematic dependence on initial tube parameters. Particularly at high latitudes and high field strengths the flow instability is responsible for the majority of erupting flux tubes. The dependence of the evolution of flux tubes on the instability mechanism (with similar initial configurations otherwise) indicates that the formation of non-uniformities at the surface is not only a matter of the tidal forces acting during the non-linear rise of the flux tubes through the convection zone, but also affected by stability properties in the overshoot region. While the Parker-type instability is basically a buoyancy-driven mechanism and thus susceptible to perturbations of gravity and stellar structure, the flow instability is more related to the tube parameters, namely its diameter and the relative velocity perpendicular to the environment.

For some ( $B_s, \lambda_s$ ) combinations the set of erupting flux tubes does not yield a continuous function  $\phi_e(\phi_s)$  like the ones shown in Fig. 5. Instead, they yield either piecewise steady functions, which frequently alternate between two branches or irregular distributions, which show no obvious relation to the original shift of perturbation longitudes,  $\phi_s$ . These particular configurations with irregular distributions are limited to  $B_s \gtrsim 1.5 \cdot 10^5$  G,  $\lambda_s \approx 15 \dots 35^\circ$ , a parameter domain mainly showing a Parker-type instability with  $m = 2$ , which roughly coincides with the region of retarded flux eruption described in Sect. 4.1. Because of the dominating unstable wave mode with  $m = 2$ , two loops of similar size form at opposite sides of the initially toroidal flux tube in the overshoot region and enter the convection zone, whereby the wave-like character of the instability causes a longitudinal propagation. Non-linearities lead to slightly different evolutions of the two loops, so that the early stage of the development is characterised by consecutive changes of the dominance between both loops until one of them prevails and eventually emerges. In this stage, the time delays of rising flux loops described above entail longitudinal offsets owing to their wave-like propagation. Flux tubes starting with different values  $\Delta\phi_s$  may suffer different time delays before they resume their rise and emerge at the surface. The originally continuous phase shift  $\Delta\phi_s$  imprinted on a set of flux

tubes is thus annihilated and the resulting longitudinal distribution irregular. Since for any  $(B_s, \lambda_s)$  configuration only twenty simulations (per semi-hemisphere) are accomplished, the irregular distributions can however exhibit non-uniformities due to the small statistical sample. For a large number of simulations we would expect a rather uniform distribution.

The trajectories of rising flux tubes exhibit the poleward deflection typical for fast rotators, which is caused by the dominance of the Coriolis force over the buoyancy force (Schüssler & Solanki 1992). The latitudinal deflection leads to an overlap of patterns of erupting flux tubes with different initial latitudes, which results in a superposition of clusters at different longitudes thus broadening the range of preferred longitudes in the surface distributions. The deflection is largest for flux tubes starting at equatorial and low latitudes and decreases for intermediate and high initial latitudes. An explanation for the observed high-latitude and polar spots in the framework of the present erupting flux tube model thus requires large amounts of magnetic flux at high latitudes in the overshoot region, either generated by a suitable dynamo mechanism or transported by large-scale motions inside the convection zone. Alternatively, flux erupting at lower latitudes may be transported toward the pole by meridional motions (Schrijver & Title 2001).

The investigation of binary systems with different orbital periods, i.e., distance between the components, shows that the non-uniformities become more pronounced with stronger tidal effects. The orbital period of about  $T \sim 5$  d for the onset of clustering is in agreement with the results from Heckert & Ordway (1995). In general, the non-uniformities increase for smaller orbital periods, but this trend is accompanied by a transition from clusters localised in narrow longitudinal intervals to broader intervals, up to major fractions of the stellar circumference. The number of cases with irregular longitudinal distributions increases for smaller orbital periods. This is in accordance with our interpretation that, with a closer proximity of the companion star, the resonant interaction between the tube and the tidal effects becomes more efficient and eventually ends up in an analogy to the ‘resonant catastrophe’ of a driven oscillator.

The action of tidal effects on the dynamics of magnetic flux tubes is basically a *cumulative* effect, which proceeds and adds up during the entire rise from the overshoot region up to the surface. During this time, an individual flux tube is subject to further interactions with, e.g., turbulent convective motions, differential rotation, meridional flows, and with other concentrations of magnetic flux. Although these additional interactions may modify the evolution and alter the final location of eruption to some extent, we do not expect them to severely diminish the characteristic *non-axisymmetric* influence of the companion star since they are presumably axisymmetric on average. However, it should be kept in mind that the applied thin flux tube model represents a rough simplification of the magnetic field structure in convective stellar envelopes.

The distributions of flux eruption shown above allow *statistical* predictions, which apply to large numbers of erupting flux tubes with similar initial configurations. Our simulations are based on flux tubes evenly distributed in latitude as well as on perturbations evenly distributed in longitude.

A changing situation in the overshoot region, e.g., a dependence of the amount of magnetic flux on latitude due to a particular dynamo mechanism or a dependence of tube perturbations on longitude due to a dependence of convective motions on tidal effects, could, in principle, be taken into account by folding the specific initial condition with the present non-linear mapping of rising flux tubes from the bottom of the convection zone to the top. Although the frequently observed occurrence of spot clusters at opposite sides of stellar hemispheres can consistently be explained by the dominance of the  $\pi$ -periodic contributions of tidal effects, our time-independent patterns of emergence do not immediately allow a description of the frequently observed azimuthal migration of spot clusters in time (Strassmeier 1994; Rodonò et al. 1995, 2000; Berdyugina & Tuominen 1998). However, a non-stationary dynamo mechanism with latitudinal propagation of a dynamo wave would lead to a time- and latitude-dependent field strength and magnetic flux, so that the systematic dependence of the cluster longitudes on field strength shown in Fig. 7 could transform into a longitudinal migration of the spot clusters in time.

We considered a binary system with two solar-type main sequence components to investigate the basic effects of tidal interaction on the evolution of erupting flux tubes. Although the results shown here are consistent with some observations, there are observed spot properties which are not explained by our results, like spots at very low latitudes or fixed spot clusters around the substellar point (Lanza et al. 2001, 2002; Oláh et al. 2002). RS CVn systems, however, typically consist of at least one (sub-)giant component with a much deeper convective envelope than the Sun, leading to the assumption that the formation and orientation of spot clusters are not exclusively dependent on the binary separation alone, but also in a more complicated way on the type and structure of the star. The deep convection zone of a giant, for example, will probably modify the properties of patterns of eruption owing to the cumulative character of the interaction between the rising flux tube and the companion star.

## 6. Conclusion

Erupting flux tubes in binary stars are considerably affected by the tidal influence of the companion star. Although the magnitude of tidal effects – the tidal force and the deviation of the stellar structure from spherical symmetry – are rather small for the systems considered here, they are capable to alter the surface distributions of erupting flux tubes. This results in clusters of emerging flux tubes at preferred longitudes and in the formation of spot clusters on opposite sides of the active component. We consider two main reasons for this behaviour:

1. Contrary to single-loop tubes, which are not strongly affected, the geometry of double-loop tubes (with azimuthal wave number  $m = 2$ ) allows of an efficient *resonant interaction* with the congruent  $\pi$ -periodic structure of the dominating tidal effects.
2. Since the rise of magnetic flux tubes from the bottom of the convection zone until eruption at the surface takes about

several months or years, the *cumulation of the tidal effects* leads to a strong influence on the resulting emergence pattern.

The distributions of erupting flux tubes shown here are based on uniformly distributed initial conditions (distributions of flux tubes and their localised perturbation inside the overshoot-region). More realistic spot distributions require the application of a dynamo model, which determines the spatial and temporal distribution of magnetic flux at the bottom of the convection zone. Furthermore, calculated surface distributions for one system cannot easily be used for other systems with different stellar or orbital parameters since changes of these quantities alter the tube evolution and patterns of emergence; individual studies have to be carried out for each system.

*Acknowledgements.* Volkmar Holzwarth thanks Prof. S. K. Solanki and Prof. F. Moreno-Insertis for valuable discussions and the Max-Planck-Institut für Aeronomie in Katlenburg-Lindau and the Kiepenheuer-Institut für Sonnenphysik in Freiburg/Brsg. for financial support during the accomplishment of this work.

## References

- Berdyugina, S. V., Berdyugin, A. V., Ilyin, I., & Tuominen, I. 1998, *A&A*, 340, 437
- Berdyugina, S. V. & Tuominen, I. 1998, *A&A*, 336, L25
- Caligari, P., Moreno-Insertis, F., & Schüssler, M. 1995, *ApJ*, 441, 886
- Ferriz-Mas, A. & Schüssler, M. 1995, *Geophys. Astrophys. Fluid Dyn.*, 81, 233
- Heckert, P. A. & Ordway, J. I. 1995, *Astron. J.*, 109, 2169
- Henry, G. W., Eaton, J. A., Hamer, J., & Hall, D. S. 1995, *ApJS*, 97, 513
- Holzwarth, V. & Schüssler, M. 2000, *Astron. Nachr.*, 321, 175  
—, 2003, *A&A*, submitted
- Jetsu, L. 1996, *A&A*, 314, 153
- Lanza, A. F., Catalano, S., Rodonò, M., et al. 2002, *A&A*, 386, 583
- Lanza, A. F., Rodonò, M., Mazzola, L., & Messina, S. 2001, *A&A*, 376, 1011
- Moreno-Insertis, F. 1986, *A&A*, 166, 291
- Oláh, K., Strassmeier, K. G., & Weber, M. 2002, *A&A*, 389, 202
- Rodonò, M., Lanza, A. F., & Catalano, S. 1995, *A&A*, 301, 75
- Rodonò, M., Messina, S., Lanza, A. F., Cutispoto, G., & Teriaca, L. 2000, *A&A*, 358, 624
- Schrijver, C. J. & Title, A. M. 2001, *ApJ*, 551, 1099
- Schüssler, M., Caligari, P., Ferriz-Mas, A., Solanki, S. K., & Stix, M. 1996, *A&A*, 314, 503
- Schüssler, M. & Solanki, S. K. 1992, *A&A*, 264, L13
- Spruit, H. C. 1981, *A&A*, 102, 129
- Strassmeier, K. G. 1994, *A&A*, 281, 395
- Strassmeier, K. G., Hall, D. S., Fekel, F. C., & Scheck, M. 1993, *A&AS*, 100, 173